International Immunopharmacology 117 (2023) 109960

Contents lists available at ScienceDirect

International Immunopharmacology

journal homepage: www.elsevier.com/locate/intimp

Electrochemical nanobiosensor based on reduced graphene oxide and gold nanoparticles for ultrasensitive detection of microRNA-128

Javad Mohammadnejad [a,*], Niki Basirhaghighi [a], Fatemeh Yazdian [a,*], Mehrab Pourmadadi [b], Javad Shabani shayeh [c], Meisam Omidi [c], Mojdeh Mirshafiei [b], Abbas Rahdar [d,*], Ana M. Díez-Pascual [e,*]

[a] Department of Life Science Engineering, Faculty of New Sciences and Technologies, University of Tehran, Tehran 14395-1561, Iran
[b] Department of Biotechnology, School of Chemical Engineering, College of Engineering, University of Tehran, Tehran, Iran
[c] Protein Research Center, Shahid Beheshti University, G. C., Velenjak, Tehran, Iran
[d] Department of Physics, Faculty of Science, University of Zabol, 538-98615 Zabol, Iran
[e] Universidad de Alcalá, Facultad de Ciencias, Departamento de Química Analítica, Química Física e Ingeniería Química, Ctra. Madrid-Barcelona, Km. 33.6, 28805 Alcalá de Henares, Madrid, Spain

ARTICLE INFO

Keywords:
Electrochemical nanobiosensors
Methylene blue
Hexacyanoferrate
microRNA
Leukemia, Real sample

ABSTRACT

Acute lymphoblastic leukemia (ALL) is one of the most prevalent cancers in children and microRNA-128 is amongst the most useful biomarkers not only for diagnosis of ALL, but also for discriminating ALL from acute myeloid leukemia (AML). In this study, a novel electrochemical nanobiosensor based on reduced graphene oxide (RGO) and gold nanoparticles (AuNPs) has been fabricated to detect miRNA-128. Cyclic Voltametery (CV), Square Wave Voltametery (SWV) and Electrochemical Impedance Spectroscopy (EIS) have been applied to characterize the nanobiosensor. Hexacyanoferrate as a label-free and methylene blue as a labeling material were used in the design of the nanobiosensors. It was found that the modified electrode has excellent selectivity and sensitivity to miR-128, with a limit of detection of 0.08761 fM in label-free and 0.00956 fM in labeling assay. Additionally, the examination of real serum samples of ALL and AML patients and control cases confirms that the designed nanobiosensor has the potential to detect and discriminate these two cancers and the control samples.

1. Introduction

Despite remarkable developments in medical science, cancer remains one of the main diseases of the century. According to the Leukemia and Lymphoma society report, every three minutes, a person is diagnosed with leukemia [1,2]. Leukemia is the most common cancer in children and it is divided into 4 subgroups ALL, AML, CLL, and CML based on the average survival rate and morphological characteristics [3]. The most prevalent childhood cancer is acute lymphoblastic leukemia (ALL), while acute myeloid leukemia (AML) is commonly diagnosed in adults [4]. Since the therapeutic and prognosis procedures differ between ALL and AML; ALL should be differentiated from AML at diagnosis [5]. There are various biomarkers in cancer that can be used in early diagnosis.

In humans more than 1000 miRNAs have been identified that can target more than 30 % of the human genome. miRNAs are small conserved RNA molecules with 18–25 bp, which can regulate gene expressions in the post-transcriptional phase [6] by pairing with a target mRNA [7]. involved in cell development, growth and differentiation, apoptosis, and tumorigenesis [6]. Although many studies have been conducted on the relationship between adult cancers and miRNAs, few studies have been conducted on childhood malignancies. Former studies have demonstrated that some miRNAs, such as miRNA-128, play a significant role in childhood ALL. The results confirmed that ALL could be discriminated from AML and control cases, by detecting highly increased miRNA-128 [7]. Several methods such as quantitative polymerase chain reaction (qPCR), deep sequencing, and northern blotting are currently used to detect miRNAs [8,9]. Recently, the development of biosensors for detecting leukemia has increased dramatically, offering significant advantages compared to current diagnostic methods [10,11]. Over recent years, biosensors have become widespread in medical diagnostics due to population growth and increasing chronic diseases

* Corresponding authors.
E-mail addresses: mohamadnejad@ut.ac.ir (J. Mohammadnejad), yazdian@ut.ac.ir (F. Yazdian), J_shabani@sbu.ac.ir (J.S. shayeh), m_omidi@sbmu.ac.ir (M. Omidi), a.rahdar@uoz.ac.ir (A. Rahdar), am.diez@uah.es (A.M. Díez-Pascual).

https://doi.org/10.1016/j.intimp.2023.109960
Received 2 December 2022; Received in revised form 20 February 2023; Accepted 27 February 2023
Available online 8 March 2023

[12]. World Health Organization (WHO) explains the ideal property for a diagnostic test by the acronym "ASSURED", affordable, sensitive, specific, user-friendly, rapid, equipment-free, and deliverable [13]. Biosensor detectors or transducers are based on electrochemical, optical, colorimetric, thermal, piezoelectric, and magnetic principles [14,15]. In comparison to optical sensors, electrochemical sensors are typically simple, fast, inexpensive, possible to miniaturize, and capable of being manufactured in large quantities [16]. To improve detection specificity and sensitivity, nanomaterials are used in biosensors [17]. Signal amplification and generation in biosensors can be significantly improved [18] upon incorporation of nanomaterials such as graphene, carbon nanotubes (CNTs), metal nanoparticles and quantum dots [2], due to the unique chemical and physical properties [19,20].

In the present study, an electrochemical nanobiosensor based on graphene derivatives with gold has been designed to detect miRNA-128 in ALL cancer. In electrochemical biosensors, the kinetics of the reaction on the biosensor interface is directly related to the surface properties [21,22]. Hybrid nanomaterials with diverse components can induce better performances [23].

Graphene, a 2D allotropic form of carbon, has outstanding characteristics including low electrical resistivity ($\approx 10^{-8}$ Ω·m) [24], very high surface area (2.630 $m^2.g^{-1}$), high intrinsic electron mobility (200000 $cm^2.V^{-1}.s^{-1}$), high optical transmittance (~97.7 %) [25] and good biocompatibility [26]. Reduced graphene oxide (RGO) is one of the graphene derivatives that can be obtained via reduction of graphene oxide (GO), and it incorporates a few oxygenated functional groups such as C–OH, C–O–C, C = O, and O = C–OH, which provide superior functions such as proton conductivity, catalytic activity, and selective absorption. Further, RGO can considerably increase the graphene surface, thus leading to better interaction with oligonucleotides [27]. Gold combined with graphene derivatives can enhance signal amplification and immobilize the thiolated oligonucleotides on the carbon surface.

The aim of this study is to detect miRNA-128 by hybridization with a complementary sequence on the biosensor. The hybridization of two strands of oligonucleotides in electrochemical biosensors must be demonstrated with a signal. Biosensors often require labels attached to the targeted analyte to attain a sensitive detection. As a result, the final sensor signal corresponds to the amount of labels. Label indicators like methylene blue, metal, or enzyme complexes can be used in hybridization tracing. On the other hand, label-free techniques are suitable for targeted molecules that are not labeled or the screening of analytes that are not easy to tag. They have no indicators and this strategy can overcome the disadvantages of probe labeling [28–30]. In the current study, label-free and labeling methods with methylene blue were applied, in order to compare the results obtained from both approaches.

In biosensors, the most common sample for testing is serum [31]. Advantages of human body fluid samples over tissues for disease diagnosis include low invasiveness, low cost, and rapid sample collection. In this research, synthetic miRNA-128 was spiked in serum samples at five different concentrations. 5 new cases of childhood ALL (2–7 years old), 3 new cases of childhood AML (10–11 years old), which have been approved by RT-PCR and flow cytometery, and 6 control cases (2–12 years old) were used for detecting miRNA-128 with the developed nanobiosensor. To the best of our knowledge, no previous articles on the development of electrochemical biosensors to detect microRNA-128 or specific biomarkers to distinguish between ALL and AML have been reported. In this work, a simple, sensitive, selective, rapid, cost-effective, detection of miRNA-128 is reported. Also, no former studies have compared serums of ALL, AML and control cases with electrochemical nanobiosensors.

2. Experimental

2.1. Reagents and materials

Analytical graphite powder, sulfuric acid (H_2SO_4), potassium permanganate ($KMnO_4$), hydrochloric acid (HCl), sodium borohydride ($NaBH_4$), ethanol (C_2H_5OH), tetrachloroauric acid ($HAuCl_4{\cdot}6H_2O$), potassium hexacyanoferrate (II) ($K_4[Fe(CN)_6]$), Fetal Bovine Serum (FBS) and glucose were all purchased from Sigma-Aldrich. Double-distilled water was used to prepare all solutions.

2.1.1. Oligonucleotides

Thiolated probe and two non-complementary sequences used in this study were purchased from BioBasic (Canada) and miRNA-128 sequence from Microsynth (Switzerland), respectively. All the sequences were purified by HPLC and 5OD.

Sequences are listed as follows:

Thiolated probe: 5′- AAAGAGACCGGTTCACTGTGA −3′ (3′reduced –SH).

miRNA-128: 5′-UCACAGUGAACCGGUCUCUUU-3′.

Non-complementary sequence 1:

5′-CTTCTGCCCGCCTCCTTCCTAGCCGGATCGCGCTGGCCAGATGA-TATAAAGGGTC AGCCCCCCAGGAGACGAGATAGGCGGACACT-3′.

Non-complementary sequence 2:

non-complementary sequence 2:

5′-TTTTTTTTTTATTAAAGCTCGCCATCAAATAGCTGC-3′.

2.2. Procedures:

2.2.1. Fabrication of graphene oxide

Graphene oxide (GO) was synthesized from graphite powder following the Hummeŕs method. A brief explanation of the method is as follows: 1 g of graphite powder was added to 20 ml of sulfuric acid (98 %) in an ice bath under stirring. After it was completely dissolved, 3 g of $KMnO_4$ was slowly added to the mixture under stirring at 8 °C. During this step the mixture color turned to yellow-green. After 1 h, 50 ml of deionized water was added dropwise, and then another 100 ml was added. Subsequently, the mixture was treated with 35 ml of H_2O_2, which was added gradually to neutralize the $KMnO_4$. After 18 h of stirring, the mixture was centrifuged at 4000 rpm and the remaining undissolved substances were treated with 5 % HCl. To ensure that no excess materials remained in the solution, this step was repeated four times. Finally, the graphene oxide was dried in an oven (150 °C/ 2 h).

2.2.2. Preparation of reduced graphene oxide from graphene oxide

0.6 g of the graphene oxide prepared in the previous step was dissolved in 100 ml of deionized water and then probe sonicated for 10 min until the graphene oxide particles were completely homogeneous. In the next step, 1 g of $NaBH_4$ was added dropwise to the mixture. The resulting solution was completely dried at 100 °C for 24 h. The dried material was then washed with deionized water and ethanol and the obtained precipitate was placed in an oven at 80 °C overnight. The resulting powder was RGO.

2.2.3. Synthesis of RGO-Au

0.35 g of RGO was added to 80 ml of deionized water and dissolved completely with an ultrasonic bath. Then, 2 ml of 0.25 M $HAuCl_4{\cdot}6H_2O$ was added dropwise and the mixture was kept under stirring for 3 h at room temperature. Finally, the sediment was collected, treated with deionized water and ethanol, and dried at room temperature.

2.2.4. Probe Immobilization, hybridization with miRNA-128, labeling and electrochemical measurements

First, 6 mg/mL of RGO-Au was prepared. Subsequently, 98 uL of the RGO-Au was mixed with 2 uL of the thiolated 3′end probe and incubated at 4 °C (refrigeration temperature) for 18 h. This temperature was chosen to enhance the interaction between rGO/Au and the aptamer. Self-assembled monolayers (SAMs) were formed through tight bonds between gold and thiol (Au-S) [32]. Afterward, 18 uL of this solution was added to 2 uL of nafion at room temperature to improve the affinity of the materials on GCE [33]. Nafion also induces a better dispersion of

graphene in aqueous solution and can boost the stability of graphene on the biosensor surface [34]. After 15 min, 6 uL of the mixture were dropped on the GCE surface which was rubbed by alumina powder. After drying the mixture, GCE was rinsed with PBS (pH = 7.4) to remove the excess of ss-DNA that was not adsorbed on the surface. In the tests that used methylene blue, the electrode was floated in methylene blue for 1 h after the RGO/Au/Probe was dropped on the surface. Hybridization was performed by placing 10 ul of the miRNA-128 on the modified GCE. Once the hybridization was accomplished, the GCE was rinsed with PBS to remove the excess single strand miRNAs. Eventually, the electrochemical response was measured with CV, SQW and EIS. Scheme 1 depicts the steps for the synthesis of the nanobiosensor, from graphene oxide preparation to the electrochemical measurements.

2.2.5. Characterization of produced nanomaterials

To confirm the quality of the synthesized nanomaterials, they were characterized by different techniques. Transmission electron microscopy (TEM) (Zeiss, EM10C, 80 kV, Germany) was used to assess the surface morphology and size of RGO/AuNPs. To get insight about the crystalline structure of GO and RGO/AuNPs, X-ray diffraction (XRD) (STOE, Germany) was applied with a Cu-Kα monochromatized radiation source and a Ni filter. Also, FTIR spectra (Thermo Incol, USA) were obtained to characterize GO, RGO/AuNPs and RGO/AuNPs/Probe. Electrochemical experiments were performed with a potentiostat/galvanostat device (Ivium technologies. Netherlands) using a ferrocyanide redox probe (0.2 mM) and PBS 0.1 M. A three-electrode system (Detect, Iran) comprising a working electrode (2 mm diameter glassy carbon electrode), a reference electrode (Ag/AgCl electrode), and a counter electrode (platinum) was utilized.

3. Results and discussion

3.1. Characterization of synthesized materials

To assess the surface morphology of the synthesized RGO-Au, TEM images were recorded, and typical images are shown in Fig. 1 (A). A uniform single layer of RGO and the attached Au nanoparticles individually dispersed on the RGO can be observed. The NPs are spherical, with a diameter smaller than 100 nm. RGO modification with AuNPs increased the conductivity and the nanoparticles provided an excellent surface for self-assembling the thiolated probe.

To investigate the functional groups of the synthesized materials, FTIR was used. In the FTIR of graphene oxide (Fig. 1(B)), a large peak is found at 3355 cm^{-1} indicating the O–H group. RGO-Au and RGO-AuNPs-Probe also show large peaks at 3359 and 3439 cm^{-1}, respectively, corresponding to the same functional group. In addition, the absorption peaks at 1610 and 1710 cm^{-1} are assigned to C–C and C = O bonds, respectively, and those at 1040 and 1220 cm^{-1} can be related to C-O bonds. It is clear that the intensity of the peak at 3359 cm^{-1} in RGO-Au is significantly lower compared to that of graphene oxide. Also in this material, the reduction in the intensity of the peak corresponding to C = O functional groups may be due to the bonding of these groups to gold atoms. Additionally, in the spectrum of RGO-Au, a new peak is observed in the region around 660 cm^{-1}, which corresponds to the Au-O-Au stretching. These observations corroborate the successful conversion of GO to RGO as well as the attachment of AuNPs to RGO to form the desired system. In the probe spectrum, the peak of C = O is also weakened, indicating the attachment of a number of probe molecules to these functional groups. Consequently, it is confirmed that the probes link to RGO-Au by binding the thiol functional group to gold.

In the XRD of graphene oxide (Fig. 1(C)), a peak can be observed at $2\theta = 9.91^{\circ}$, which is characteristic of this nanomaterial. For RGO-Au, the main peaks are observed at 2θ values of 38.14°, 44.32°, 64.68° and 77.50°, related to the (1 1 1), (2 0 0), (2 2 0), and (3 1 1) crystalline planes of face centered cubic gold. The peak at $2\theta = 9.91^{\circ}$ also decreased in RGO-Au, indicating the reduction process. It should be noted that peaks in the 2θ range of 15–30 ° correspond to irregular RGO sheets.

The electrochemical characterization was performed by CV and EIS techniques, and the results are shown in Fig. 2 (A) and (B), respectively. CV is the most effective and appropriate method for studying the characteristics of electrochemical processes on electrode surfaces [35], and EIS indicates the surface resistance.

CV was performed at a scan rate of 50 $mV.s^{-1}$ from −0.5 to 0.7 V and EIS was performed in the frequency range of 0.01–100000 Hz with 32 point per decade. Due to the signal amplification properties of the gold nanoparticles, the signal of RGO-Au was higher than that of the bare electrode. Probe immobilization and nafion addition increased the resistance and the signal was reduced. Subsequently, by adding miRNA-128 on the surface, the signal decreased, indicating the successful hybridization with the probe.

3.2. Biosensor time profiles optimization

One of the most important parameters in nanobiosensors is to adhere the receptor to the surface for analyte detection, which is directly affected by time. In other words, time is a crucial factor in optimizing biosensor performance since a delay in the biosensor response time prevents timely action. The time period determines the amount of probe

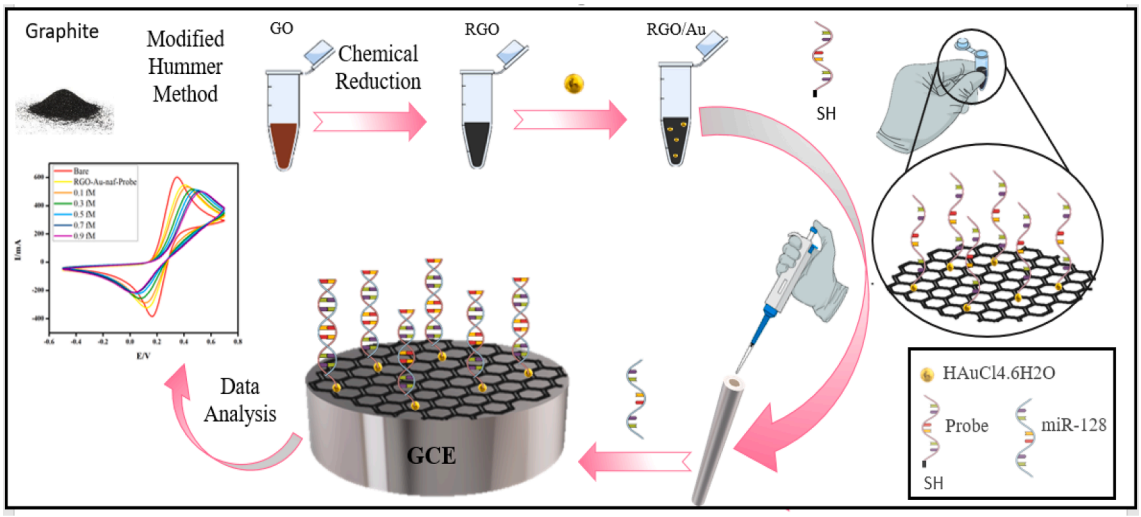

Scheme 1. Representation of the fabrication of the electrochemical miRNA nanobiosensor.

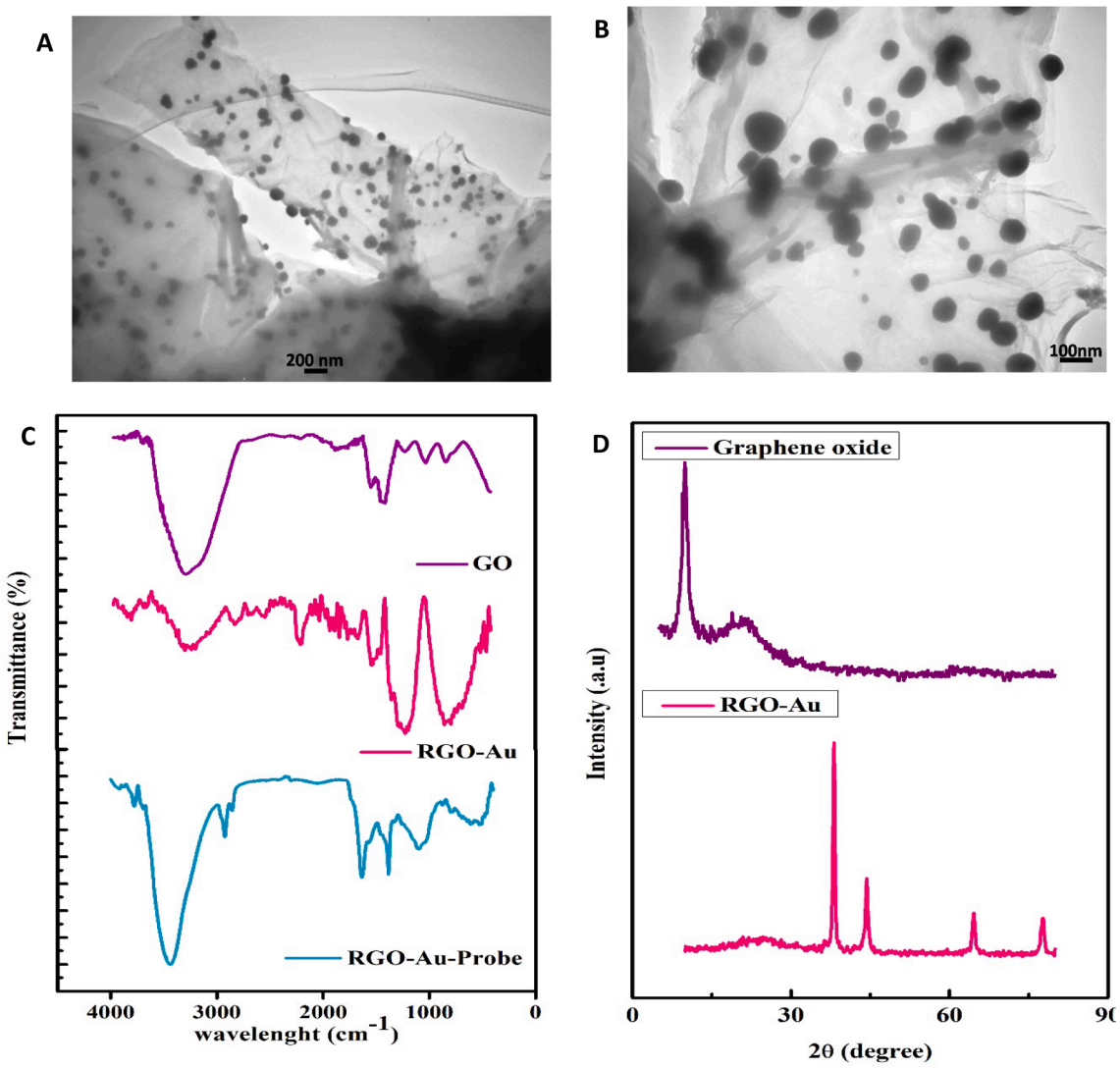

Fig. 1. (A) and (B) TEM micrographs of RGO/AuNPs showning a uniform single layer of RGO and the attached Au NPs well dispersed on RGO with a diameter smaller than 100 nm. (C) FTIR spectra of GO, RGO/AuNPs and RGO/AuNPs/probe and (D) XRD pattern of GO and RGO/AuNPs.

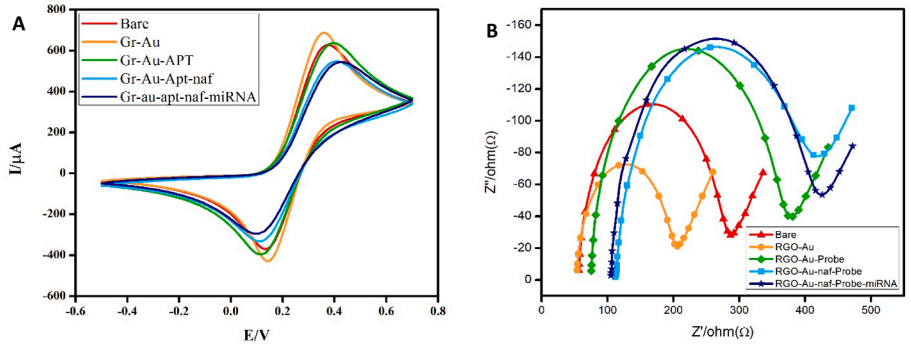

Fig. 2. Electrochemical characterization via (A) CV and (B) EIS analysis of Gr-Au, Gr-Au-APT, Gr-Au-Apt-naf, Gr-Au-Apt-naf-miRNA in hexacyanoferrate (labeled sensor). CV was analyzed in the range of −0.5 to 0.7 V.

attached to gold. The 3′thiolated probe could be immobilized by self-assembling to the gold nanoparticles via Au-S bonds. These bonds aid probes to get a proper orientation on the fabricated nanobiosensor which is necessary for improving the detection sensitivity [36]. Therefore, in order to attain the maximum probe immobilization, experiments were performed at 4 ℃ for incubation times of 6, 12, 18, and 24 h in ferrocyanide, as shown in Fig. 3 (A). The figure shows that an incubation period of 18 h was found to be optimal for immobilizing probes.

The hybridization of the probe and miRNA-128 also depends on time. For this purpose, the hybridization was measured in ferrocyanide at 0, 10, 20, 30, 40, 50, and 60 min. The signal significantly increased up to 40 min and then remained constant. Fig. 3 (B) shows that the optimal

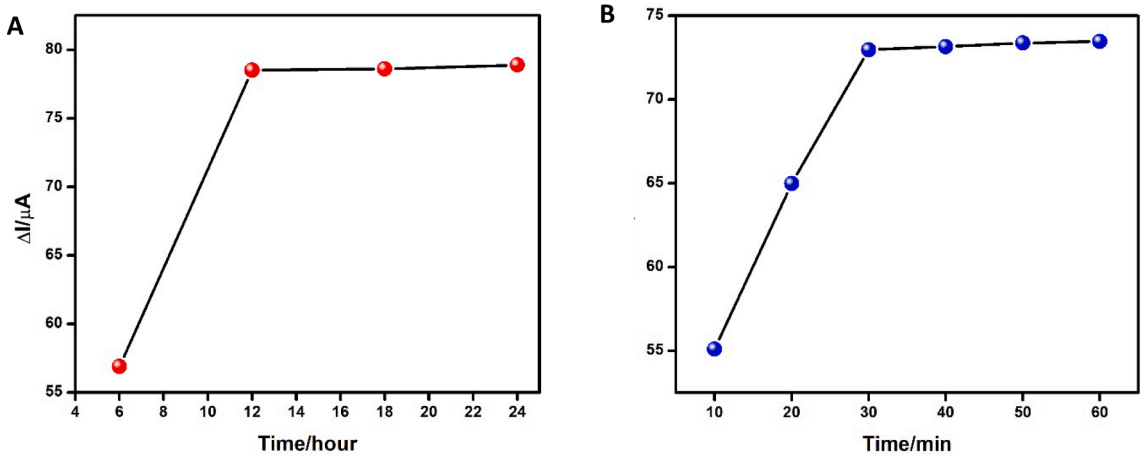

Fig. 3. Time diagram (A) for the hybridization of the probe and microRNA-128. (B) for the immobilization of the probe with AuNPs.

hybridization period was 40 min.

3.3. Electrochemical characterization of modified electrode with label-free method

The label-free electrochemical characterization of GCE/RGO/AuNPs/Probe electrode was performed by SWV and EIS in ferrocyanide solution $[Fe(CN)_6]^{-3/-}4$, and the results for different microRNA-128 concentrations are shown in Fig. 4 (A) and (B), respectively. The corresponding calibration curves are depicted in Fig. 4 (C) and (D), respectively. This method measured SWV between −0.2 and 1 V. As shown in Fig. 4(A), the peak intensity decreased with increasing miRNA concentration. Further, a perfect linear relationship was found between the resistance and the concentration of microRNA-128.

3.4. Characterization of the labeling modified electrode by methylene blue

Methylene blue (MB) is one of the redox indicators used in biosensors as a label. MB has a high capability to interact with high guanine-cytosine content of single-strand DNA (ss-DNA) and double-strand

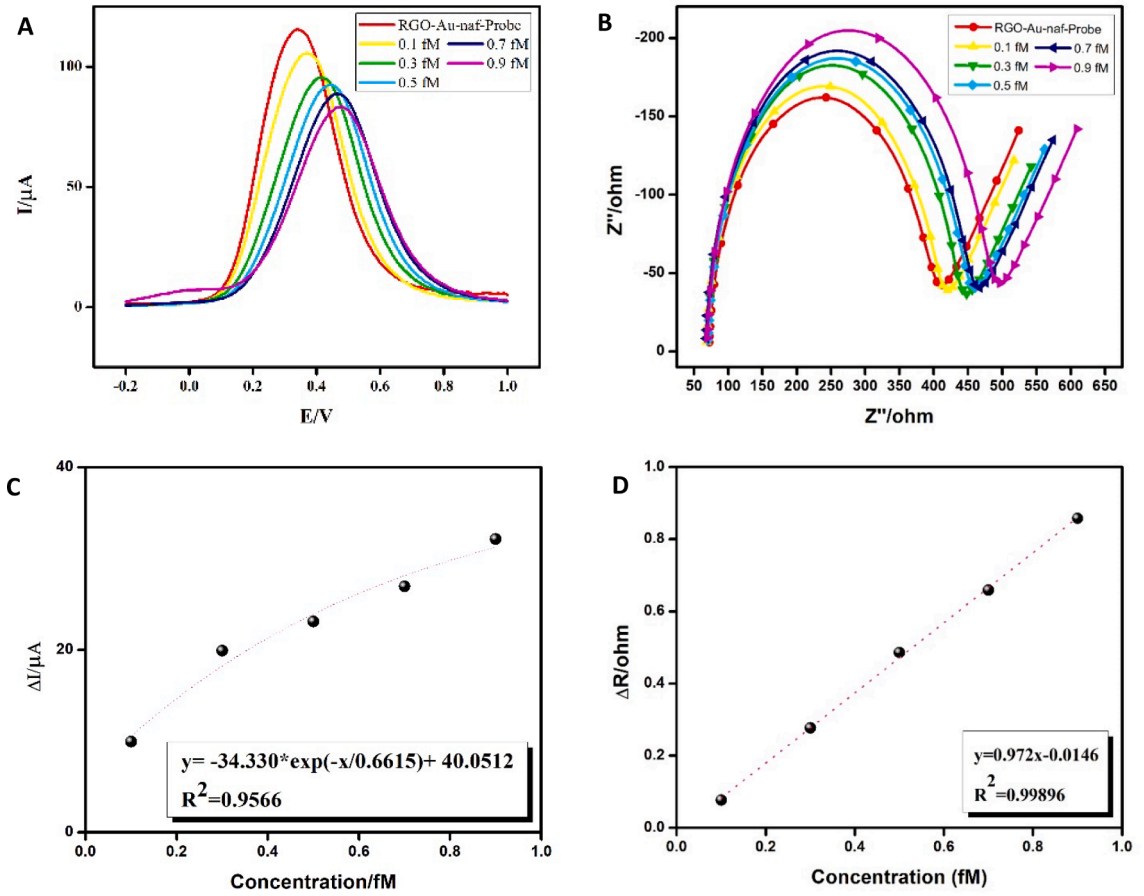

Fig. 4. A) SWV and (B) EIS plot of GCE/RGO/AuNPs/Probe electrode in hexacyanoferrate for different microRNA-128 concentrations. Calibration curve obtained from SWV (C) and (D) EIS results.

DNA (ds-DNA) by electrostatic adsorption [37]. In this work, after preparation of the electrode with RGO/Au/Probe, the electrode was rinsed in methylene blue. MB intercalated between the nucleic acids of the probe and acted as a redox indicator. After washing the remaining MB, stability was evaluated using 30 cycles of CV in PBS, in the potential range from 0 to −0.4 V. The high stability of methylene blue in the biosensor is demonstrated in Fig. 5 (A).

Furthermore, the diffusion control of methylene blue in Fig. 5 (B) was examined with CV at scan rates of 10, 15, 25, 50, 75, 100, 125, 150, 200 and 300 V/s, in the potential range of −0.4–0. miRNA-128 was applied on the RGO-Au/nafion, and SWV was carried out from 0 to −0.4 V. Fig. 5 (C) clearly shows that the SWV peak decreases with increasing the concentration of miRNA-128.

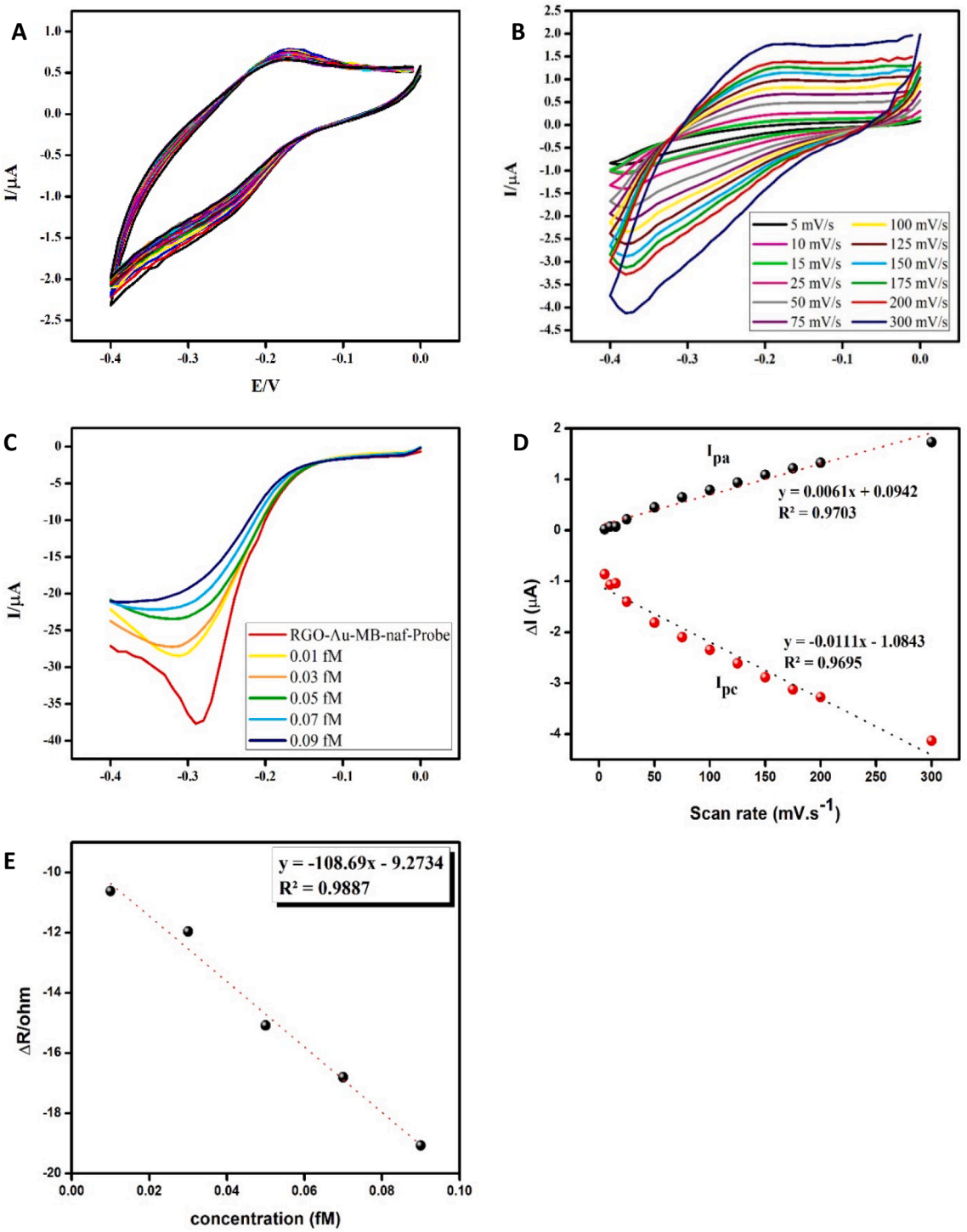

Fig. 5. (A) Stability diagram of methylene blue on modified GCE with RGO/AuNPs/Probe in PBS medium. (B) diagram of methylene blue at different scan rates. (C) CV analysis of methylene blue assay for different microRNA-128 concentrations. (D) Calibration curve of methylene blue as a function of the scan rate. (E) Calibration curve obtained from CV analysis of methylene blue assay vs. microRNA-128 concentration. (For interpretation of the references to color in this figure legend, the reader is referred to the web version of this article.)

3.5. Analytical performance of quantitative detection of miRNA-128

Square wave voltammetry (SWV) is widely used to study changes in the DNA hybridization. The label-free (ferrocyanide) and labeled (methylene blue) nanobiosensors were used to quantitatively detect miRNA-128 at concentrations in the range of 0.1–0.9 fM and 0.01–0.09 fM, respectively. Under optimal conditions, the LOD of the label-free method was 0.8761 fM and for the methylene blue assay was 0.00951 fM. It is clear that the LOD of the methylene blue assay is much lower than that of the label-free method. This means that labeled assays have higher selectivity than label-free methods. Table 1 compares the results of this study with those of previous literature reviews.

In the EIS diagram, the resistance and electrical conductivity of the electrode are both reduced as the target analyte is connected to the electrode. While the linear segment at low frequencies represents the propagation phenomenon, the semicircular segment at high frequencies represents electron transfer. By studying the impedance spectrum, it is possible to identify the specific interaction at the electrode surface that affects the resistance of the electrode to transient current. The spectra are presented in the form of Nyquist plots (Fig. 4B). The increase in Rct (the larger the radius of the semicircle the higher Rct value) with increasing analyte concentration indicates higher resistance, corroborating that the analyte was successfully captured on the electrode surface.

3.6. Selectivity of biosensor

To investigate the selectivity of the biosensor, RGO-Au/nafion/probe in ferrocyanide electrolyte was used to hybridize with FBS, glucose (90 mg/dl, fasting concentration of glucose in blood), two aptamer sequences, and miRNA-128, and their percentage of response is shown in Fig. 6. The response of miRNA-128 was significantly higher than those of the other substances (approximately 3.67 % for FBS, 12.99 % for glucose, 26.97 % for APT1, and 28.72 % for APT2 compared to the miRNA-128). The results demonstrated excellent selectivity, indicating that the prepared biosensor can differentiate miRNA-128 from other substances with high sensitivity and specificity.

3.7. miRNA spiking in SBF

miRNA spiking was investigated in simulated body fluids (SBF). This serum contains various interfering substances such as ions, with an ionic concentration close to human plasma. Five concentrations (0.1–0.9 fM) of synthetic miRNA-128 were used in SBF and SWV assays were performed with ferrocyanide. As shown in the SWV curve (Fig. 7A), the peak height decreases upon increasing miRNA-128 concentration. On the other hand, the calibration curve of the spiked concentration of miR-128 in SBF is exponential over the concentration range studied (Fig. 7B).

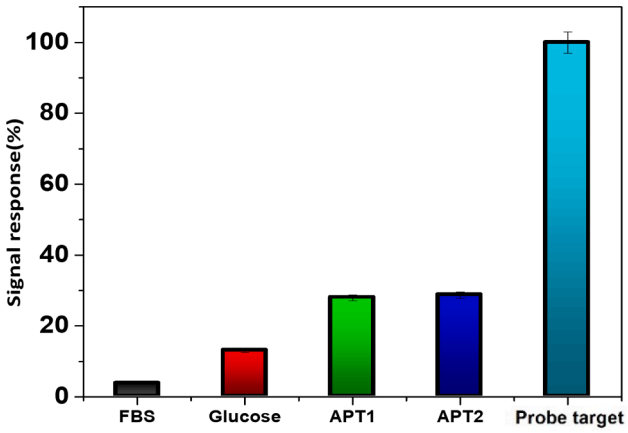

Fig. 6. Comparison of the probe selectivity to FBS, glucose (90 mg/ml), APT1, APT2 and micro-RNA-128. The sensor has higher selectivity to the miRNA-128 compared with the other materials.

3.8. Real sample assay

5 new cases of ALL, 3 AML, and 6 control serum samples were used to detect miRNA-128. RT-PCR and flow cytometry tests were performed on each patient sample. Following RGO/AuNPs/Probe electrode preparation, the serum sample was dropped on the surface for 40 min, rinsed with PBS to remove the non-hybridized miRNA, and subsequently, SWV tests were performed. As shown in Fig. 8, three zones can be distinguished: ALL patients had the highest amount of miRNA-128 (red zone) and the control cases had the lowest level of miRNA-128 (green zone). AML patients were in the mid-range (grey zone). The results indicate that this nanobiosensor can discriminate ALL, AML, and control samples in different zones.

4. Conclusion

An electrochemical biosensor based on RGO-Au/Probe was developed for miRNA-128 detection. Under the optimal detection conditions, the limit of detection was 0.08761 fM in label-free and 0.00956 fM in labeling assay, indicating the higher sensitivity of the biosensor developed herein compared to those of previous studies (Table 1). Experiments reveal that the sensitivity of the labeling method with methylene blue is much higher than that of the label-free test. However, the methylene blue analysis has an additional step. Moreover, the biosensor displayed very high selectivity for miRNA-128, and can discriminate ALL from AML and real control samples. Due to the advantages of the RGO-Au/Probe biosensor, we believe that it has great potential as a platform for ALL detection in the near future.

Table 1
Comparison of the results from previous studies with the present study. **Abbreviations:** 3-(5-hydroxy-1,4-dioxo-1,4-dihydronaphthalen-2(3)-yl) propanoic acid (JUGA), 5-hydroxy-1,4-naphthoquinone (JUG), multi-walled carbon nanotube(MWCNT), silicon nanowires (SiNWs), horseradish peroxidase (HRP), graphene quantum dots (GQD), dendritic gold nanostructure (DenAu), glassy carbon electrode (GCE), cyclic enzymatic signal amplification (CESA), methylene blue (MB), quantum dot (QD).

Electrode material	miRNA	Detecting method	Labeled/ Label-free	LOD	References
Poly(JUG-co-JUGA)/o-MWCNT modified	miRNA-141	Electrochemical	Label-free	8 fM	[38]
SiNWs	Let-7b	Optical	Label-free	1 fM	[39]
HRP-GQD	miRNA-155	Electrochemical	Labeled (HRP)	0.14 fM	[40]
HRP/bio-bar-codes /DenAu/graphene/GCE	miRNA-21	Electrochemical	Labeled (HRP)	0.06 pM	[41]
CESA/template free DNA extension reaction	miRNA-196-a	Electrochemical	Labeled (MB)	15 aM	[42]
QD-labeled strip biosensor	miRNA-21	Electrochemical	Labeled	200 aM	[43]
RGO-AuNPs	miRNA-128	Electrochemical	Label-free (hexacyanoferrate)	0.08761 fM	This study
RGO-AuNPs	miRNA-128	Electrochemical	Labeled (MB)	0.00956 fM	This study

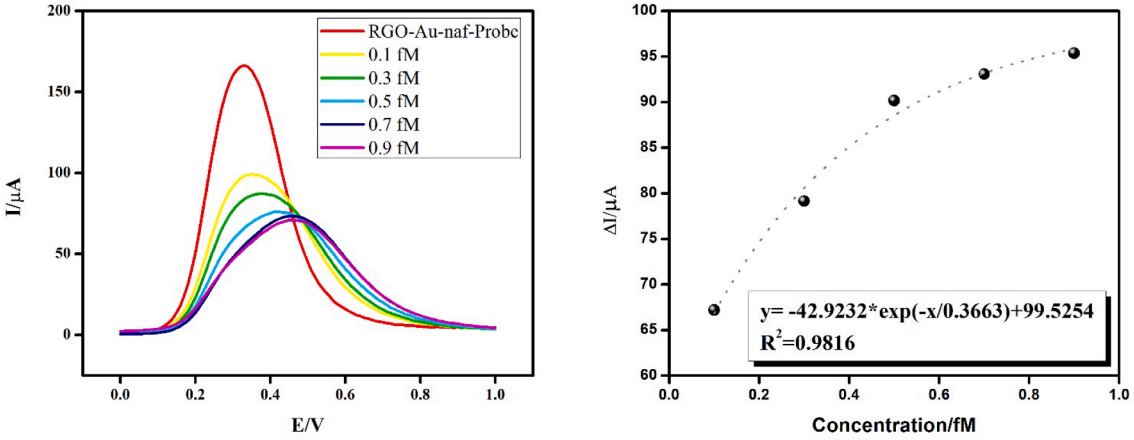

Fig. 7. (A) SWV curve and (B) calibration curve for spiked concentrations of miR-128 in SBF in hexacyanoferrate.

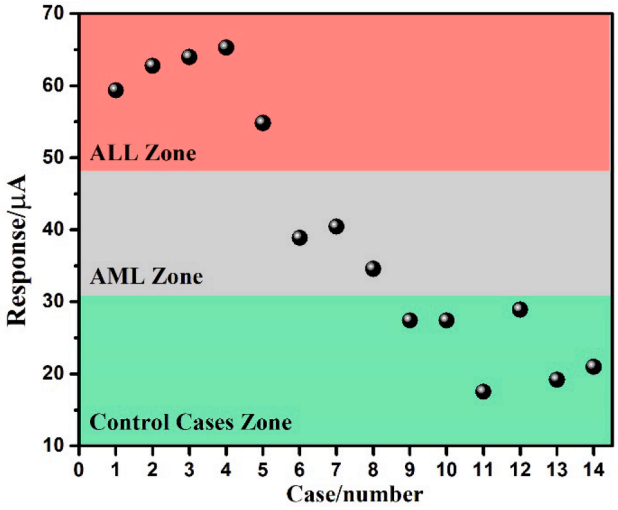

Fig. 8. Comparative diagram of the response of ALL, AML and control cases examined with SWV. The diagram can be divided into 3 sections that demonstrate the capability of the sensor for discriminating ALL, AML and control cases serums.

Funding

Financial support from the Community of Madrid within the framework of the multiyear agreement with the University of Alcalá in the line of action "Stimulus to Excellence for Permanent University Professors", Ref. EPU-INV/2020/012, is gratefully acknowledged.

Data availability statement

Data reported within this work will be available on request.

CRediT authorship contribution statement

Javad Mohammadnejad: Investigation, Formal analysis. **Niki Basirhaghighi:** Investigation. **Fatemeh Yazdian:** Supervision, Formal analysis, Methodology. **Mehrab Pourmadadi:** Writing – original draft, Writing – review & editing. **Javad Shabani shayeh:** Investigation. **Meisam Omidi:** Investigation. **Mojdeh Mirshafiei:** Investigation. **Abbas Rahdar:** Writing - review & editing. **Ana M. Díez-Pascual:** Writing - review & editing.

Declaration of Competing Interest

The authors declare that they have no known competing financial interests or personal relationships that could have appeared to influence the work reported in this paper.

Data availability

Data will be made available on request.

References

[1] J.S. Harrison, P. DesMarteau, B. Hamilton, S. Patthoff, Leukemia and lymphoma society, 2012.
[2] F. Yazdian, Aptamer-functionalized quantum dots for targeted cancer therapy, in Aptamers Engineered Nanocarriers for Cancer Therapy: Elsevier, 2023, pp. 295–315.
[3] D.L. Longo, Harrison's Hematology and Oncology, McGraw-Hill Education, 2017.
[4] L. Ries et al., SEER cancer statistics review, 1975–2005, Bethesda, MD: National Cancer Institute, vol. 2999, 2008.
[5] S. Mi et al., MicroRNA expression signatures accurately discriminate acute lymphoblastic leukemia from acute myeloid leukemia, Proc. Natl. Acad. Sci., 104, (50) (2007) 19971–19976.
[6] S. Campuzano, M. Pedrero, J.M. Pingarrón, Electrochemical genosensors for the detection of cancer-related miRNAs, Anal. Bioanal. Chem. 406 (2014) 27–33.
[7] N. Iwamoto, A. Kawakami, Recent findings regarding the effects of microRNAs on fibroblast-like synovial cells in rheumatoid arthritis, Immunol. Med. 42 (4) (2019) 156–161.
[8] R. Tavallaie, S.R. De Almeida, J.J. Gooding, Toward biosensors for the detection of circulating microRNA as a cancer biomarker: an overview of the challenges and successes, Wiley Interdiscip. Rev. Nanomed. Nanobiotechnol. 7 (4) (2015) 580–592.
[9] M. Daneshpour, B. Karimi, K. Omidfar, Simultaneous detection of gastric cancer-involved miR-106a and let-7a through a dual-signal-marked electrochemical nanobiosensor, Biosens. Bioelectron. 109 (2018) 197–205.
[10] K.Y. Avelino, R.R. Silva, A.G. da Silva Junior, M.D. Oliveira, C.A. Andrade, Smart applications of bionanosensors for BCR/ABL fusion gene detection in leukemia, J. King Saud University-Sci. 29 (4) (2017) 413–423.
[11] C. Zhu, G. Yang, H. Li, D. Du, Y. Lin, Electrochemical sensors and biosensors based on nanomaterials and nanostructures, Anal. Chem. 87 (1) (2015) 230–249.
[12] C. Choi, Integrated nanobiosensor technology for biomedical application, Nanobiosens. Dis. Diagnosis 1 (2012) 1–4.
[13] L. Duchesne, K. Lacombe, Innovative technologies for point-of-care testing of viral hepatitis in low-resource and decentralized settings, J. Viral Hepat. 25 (2) (2018) 108–117.
[14] G. Mehdipour, J. Shabani Shayeh, M. Omidi, M. Pour Madadi, F. Yazdian, L. Tayebi, An electrochemical aptasensor for detection of prostate-specific antigen using reduced graphene gold nanocomposite and Cu/carbon quantum dots, Biotechnol. Appl. Biochem. 69 (5) (2022) 2102–2111.
[15] T. Lakshmipriya, S.C. Gopinath, An introduction to biosensors and biomolecules, Nanobiosens. Biomol. Targeting: Elsevier (2019) 1–21.
[16] S. Chen, et al., Microfluidic device directly fabricated on screen-printed electrodes for ultrasensitive electrochemical sensing of PSA, Nanoscale Res. Lett. 14 (2019) 1–7.
[17] F. Saeiditabar, M. Pourmadadi, F. Yazdian, H. Rashedi, Design of a Novel Electrochemical Nanobiosensor for the Detection of Prostate Cancer by Measurement of PSA Using Graphene-based Materials, Aut. J. Electr. Eng. 53 (2) (2021) 213–222.

[18] M. Azimzadeh, N. Nasirizadeh, M. Rahaie, H. Naderi-Manesh, Early detection of Alzheimer's disease using a biosensor based on electrochemically-reduced graphene oxide and gold nanowires for the quantification of serum microRNA-137, RSC Adv. 7 (88) (2017) 55709–55719.
[19] G. Maduraiveeran, W. Jin, Nanomaterials based electrochemical sensor and biosensor platforms for environmental applications, Trends Environ. Anal. Chem. 13 (2017) 10–23.
[20] L. Syedmoradi, M. Daneshpour, M. Alvandipour, F.A. Gomez, H. Hajghassem, K. Omidfar, Point of care testing: The impact of nanotechnology, Biosens. Bioelectron. 87 (2017) 373–387.
[21] I.M. Feigel, H. Vedala, A. Star, Biosensors based on one-dimensional nanostructures, J. Mater. Chem. 21 (25) (2011) 8940–8954.
[22] F. Ostadakbari, F. Yazdian, H. Rashedi, A. Ghaemi, B.F. Haghirosadat, M. Azizi, Fabrication of a Sensitive Biosensing System for Cu 2+ ion Detection by Gold-Decorated Graphene Oxide Functionalized with Gly-Gly-His, J. Clust. Sci. (2021) 1–8.
[23] M. Holzinger, A. Le Goff, S. Cosnier, Synergetic effects of combined nanomaterials for biosensing applications, Sensors 17 (5) (2017) 1010.
[24] M. Pourmadadi, F. Yazdian, S. Hojjati, K. Khosravi-Darani, Detection of microorganisms using graphene-based nanobiosensors, Food Technol. Biotechnol. 59 (4) (2021) 496–506.
[25] Y. Zhu, et al., Graphene and graphene oxide: synthesis, properties, and applications, Adv. Mater. 22 (35) (2010) 3906–3924.
[26] C. Bosch-Navarro, Z.P. Laker, A.J. Marsden, N.R. Wilson, J.P. Rourke, Non-covalent functionalization of graphene with a hydrophilic self-limiting monolayer for macro-molecule immobilization, FlatChem 1 (2017) 52–56.
[27] F. Menaa, Y. Fatemeh, S.K. Vashist, H. Iqbal, O.N. Sharts, B. Menaa, Graphene, an interesting nanocarbon allotrope for biosensing applications: Advances, insights, and prospects, Biomed. Eng. Comput. Biol., 12 (2021) 1179597220983821.
[28] P.A. Rasheed, N. Sandhyarani, Electrochemical DNA sensors based on the use of gold nanoparticles: a review on recent developments, Microchim. Acta 184 (2017) 981–1000.
[29] M. Zamani, M. Pourmadadi, S.S. Ebrahimi, F. Yazdian, J.S. Shayeh, A novel labeled and label-free dual electrochemical detection of endotoxin based on aptamer-conjugated magnetic reduced graphene oxide-gold nanocomposite, J. Electroanal. Chem. 908 (2022) 116116.
[30] Y. Ye, et al., A label-free electrochemical DNA biosensor based on thionine functionalized reduced graphene oxide, Carbon 129 (2018) 730–737.
[31] T. Jezierski, M. Walczak, T. Ligor, J. Rudnicka, B. Buszewski, Study of the art: canine olfaction used for cancer detection on the basis of breath odour Perspectives and limitations, J. Breath Res. 9 (2) (2015) 027001.
[32] M. Pourmadadi, J.S. Shayeh, M. Omidi, F. Yazdian, M. Alebouyeh, L. Tayebi, A glassy carbon electrode modified with reduced graphene oxide and gold nanoparticles for electrochemical aptasensing of lipopolysaccharides from Escherichia coli bacteria, Microchim. Acta 186 (2019) 1–8.
[33] V. Kavita, DNA biosensors-a review, J. Bioeng. Biomed. Sci. 7 (2) (2017) 222.
[34] B. Li, et al., Sensitive HIV-1 detection in a homogeneous solution based on an electrochemical molecular beacon coupled with a nafion–graphene composite film modified screen-printed carbon electrode, Biosens. Bioelectron. 52 (2014) 330–336.
[35] M. Chen, et al., Three-dimensional electrochemical DNA biosensor based on 3D graphene-Ag nanoparticles for sensitive detection of CYFRA21-1 in non-small cell lung cancer, Sens. Actuators B 255 (2018) 2910–2918.
[36] K. Jayakumar, R. Rajesh, V. Dharuman, R. Venkatasan, J. Hahn, S.K. Pandian, Gold nano particle decorated graphene core first generation PAMAM dendrimer for label free electrochemical DNA hybridization sensing, Biosens. Bioelectron. 31 (1) (2012) 406–412.
[37] X. Miao, Z. Li, A. Zhu, Z. Feng, J. Tian, X. Peng, Ultrasensitive electrochemical detection of protein tyrosine kinase-7 by gold nanoparticles and methylene blue assisted signal amplification, Biosens. Bioelectron. 83 (2016) 39–44.
[38] H. Tran, B. Piro, S. Reisberg, L. Tran, H. Duc, M. Pham, Label-free and reagentless electrochemical detection of microRNAs using a conducting polymer nanostructured by carbon nanotubes: Application to prostate cancer biomarker miR-141, Biosens. Bioelectron. 49 (2013) 164–169.
[39] G.-J. Zhang, J.H. Chua, R.-E. Chee, A. Agarwal, S.M. Wong, Label-free direct detection of MiRNAs with silicon nanowire biosensors, Biosens. Bioelectron. 24 (8) (2009) 2504–2508.
[40] T. Hu, L. Zhang, W. Wen, X. Zhang, S. Wang, Enzyme catalytic amplification of miRNA-155 detection with graphene quantum dot-based electrochemical biosensor, Biosens. Bioelectron. 77 (2016) 451–456.
[41] H. Yin, Y. Zhou, H. Zhang, X. Meng, S. Ai, Electrochemical determination of microRNA-21 based on graphene, LNA integrated molecular beacon, AuNPs and biotin multifunctional bio bar codes and enzymatic assay system, Biosens. Bioelectron. 33 (1) (2012) 247–253.
[42] J. Guo, C. Yuan, Q. Yan, Q. Duan, X. Li, G. Yi, An electrochemical biosensor for microRNA-196a detection based on cyclic enzymatic signal amplification and template-free DNA extension reaction with the adsorption of methylene blue, Biosens. Bioelectron. 105 (2018) 103–108.
[43] H. Deng, et al., Quantum dots-labeled strip biosensor for rapid and sensitive detection of microRNA based on target-recycled nonenzymatic amplification strategy, Biosens. Bioelectron. 87 (2017) 931–940.